Geophysical Research Letters

RESEARCH LETTER
10.1029/2023GL102932

Reversible Thermal Hysteresis in Heating-Cooling Cycles of Magnetic Susceptibility: A Fine Particle Effect of Magnetite

Qi Zhang[1,2] **and Erwin Appel**[2]

[1]Center for Marine Magnetism (CM2), Department of Ocean Science and Engineering, Southern University of Science and Technology, Shenzhen, China, [2]Department of Geosciences, University of Tübingen, Tübingen, Germany

Key Points:

- We observed reversible thermal hysteresis behavior in hump-shaped partial magnetic susceptibility cycles of magnetite-bearing basalts
- The thermal hysteresis may be caused by blocked states of coupled nanoparticle moments modulating thermal activation
- Descending susceptibility in hump-shaped curves is often due to single-domain thermal relaxation rather than maghemite inversion

Supporting Information:

Supporting Information may be found in the online version of this article.

Correspondence to:

E. Appel,
erwin.appel@uni-tuebingen.de

Citation:

Zhang, Q., & Appel, E. (2023). Reversible thermal hysteresis in heating-cooling cycles of magnetic susceptibility: A fine particle effect of magnetite. *Geophysical Research Letters*, *50*, e2023GL102932. https://doi.org/10.1029/2023GL102932

Received 19 JAN 2023
Accepted 8 MAR 2023

Author Contributions:

Conceptualization: Qi Zhang, Erwin Appel
Data curation: Qi Zhang, Erwin Appel
Formal analysis: Qi Zhang, Erwin Appel
Funding acquisition: Qi Zhang, Erwin Appel
Investigation: Qi Zhang, Erwin Appel
Methodology: Qi Zhang, Erwin Appel
Project Administration: Qi Zhang, Erwin Appel
Resources: Qi Zhang, Erwin Appel
Software: Qi Zhang, Erwin Appel
Supervision: Erwin Appel
Validation: Qi Zhang, Erwin Appel
Visualization: Qi Zhang, Erwin Appel
Writing – original draft: Qi Zhang

Abstract Thermomagnetic curves of magnetic susceptibility (κ) are key to characterizing magnetic properties. We report hump-shaped κ-T curves of magnetite-bearing basalt during heating-cooling cycles to ~340°C, with a large thermal hysteresis and similar starting and ending values, even in multiple repeated cycles, ruling out changes in magnetic mineralogy. Based on FORC diagrams and published results of engineered materials, we propose that thermal hysteresis arises from configurations of magnetic moments in clusters of single-domain particles due to dipolar coupling, with different collective behavior during heating and cooling. This effect modifies the hump-shaped thermal relaxation behavior of the individual nanoparticles. FORC and κ-T results indicate an increase in effective particle sizes after 700°C-heating. Our results are a warning against premature interpretation of a decreasing trend in κ-T curves by maghemite inversion. Instead, fine particle behavior should be considered when a hump-shaped κ-T behavior is detected.

Plain Language Summary Thermomagnetic curves of magnetic susceptibility (κ) are key to characterizing magnetic properties. A marked drop in κ-T curves at ~300–400°C is often considered to indicate the inversion of maghemite to hematite. Such a drop is often preceded by an increase in κ, creating a hump shape that is rarely noted in discussions. We report hump-shaped κ-T curves in magnetite-bearing basalt. When heating up to ~340°C and cooled subsequently, a large thermal hysteresis was observed. This hump shape and the thermal hysteresis behavior occur in a very similar way in repeated κ-T cycles, ruling out changes in magnetic mineralogy. We hypothesize that the thermal hysteresis arises from configurations of coupled magnetic moments in clusters of fine particles, which is partly irreversible upon cooling. This effect modifies the hump-shaped thermal relaxation behavior of the individual particle moments. When heated to 700°C, grain boundaries may weld and internal stress effects are reduced, increasing the effective particle sizes and shifting the hump-peak to a higher temperature. Our results indicate that fine particle behavior should be considered for all types of natural materials when a hump-shaped κ-T curve is observed rather than interpreting the drop in κ as maghemite inversion.

1. Introduction

Temperature (T) variation of magnetic susceptibility (κ) is highly valuable for characterization of magnetic phases. The availability of sensitive instruments made κ-T curves extremely popular in magnetic studies. Curie temperatures and Verwey transition are easy to identify (e.g., Petrovský & Kapička, 2006; Wang et al., 2015; Zhang, Appel, Stanjek, et al., 2021), however, κ-T curves are also influenced by domain state, alteration and transformation of magnetic minerals (Deng et al., 2001; Liu et al., 2005; van Velzen & Dekkers, 1999a). Their appearance in κ-T curves is complex, and therefore interpretations are often controversial.

For magnetite-bearing samples, a decreasing trend of κ frequently appears during heating at ~300–400°C, often preceded by an increase of κ, resulting in hump-shaped heating curves. The decreasing trend is usually attributed to the inversion of maghemite to hematite (Deng et al., 2001, 2004; Dunlop & Özdemir, 1997; Liu et al., 2005; Zhu et al., 1999), or to Ti-rich titanomagnetite (Appel & Soffel, 1985; Vahle & Kontny, 2005). The κ-increase was partly interpreted as the healing of internal stresses by lowering the degree of low-temperature oxidation (LTO) or flattening of the LTO-gradient in particles (Ahmed & Maher, 2018; Dunlop, 2014; Van Velzen & Dekkers, 1999b), but more often it is simply ignored. Little attention was paid to gradual transformation of stable single-domain (SSD) to superparamagnetic (SP) behavior (Deng et al., 2000; Liu et al., 2005; Zhang et al., 2020).

In the standard procedure of κ-T cycling to ~700°C (as in Figure 1b), hump-like features appearing in heating curves are usually absent or strongly re-shaped in cooling curves (Kontny & Grothaus, 2017; Liu et al., 2005;

Writing – review & editing: Qi Zhang, Erwin Appel

Zhang, Appel, Basavaiah, et al., 2021). Recently, Zhang et al. (2020), Zhang, Appel, Basavaiah, et al. (2021) argued that hump-shaped heating curves of red soil and basalt samples represent the SSD to SP transition behavior, which is predicted by theoretical models (Egli, 2009; Worm, 1998).

In this study, we present hump-shaped κ-T curves of magnetite-bearing samples, which show a thermal hysteresis with similar heating-cooling behavior in repeated cycles, and we discuss the possible underlying mechanism of this "reversible irreversible effect."

2. Materials and Methods

We present experimental results of basalt samples (DE11, DE04) from the Deccan Traps (India) collected from weathered surfaces. Detailed rock-magnetic properties were published by Zhang, Appel, Basavaiah, et al. (2021); essential sample information is given in Supporting Information S1. Optical microscopy revealed fine lamellar magnetite-ilmenite structures with variable sizes (Figure 1a; Figures S2a and S2c in Supporting Information S1), typical for exsolution during relatively slow cooling (Ramdohr, 1980). For comparison, we also present results of a red soil sample (HQ04; southwestern China), with dominant ~5–20 nm sized pedogenic magnetite particles aggregated in clusters (Zhang et al., 2020; Figure S2b in Supporting Information S1). The basalts and the red soil showed a hump at intermediate temperatures in thermomagnetic κ-T curves during heating (Figure 1b for basalt), which Zhang et al. (2020), Zhang, Appel, Basavaiah, et al. (2021) attributed to fine particle effects.

We measured additional κ-T cycles on an MFK1-FA instrument (AGICO) at the University of Tübingen. A home-made Curie balance was used at the University of Bremen to measure saturation magnetization (M_s) (external field limited to 135 mT for a technical reason). Full (to 700°C) and partial (to ~340°C, partly higher) curves were obtained, starting from room temperature, conducted in argon (κ-T) or helium (M_s-T). First-order reversal curve (FORC) diagrams at room temperature were generated at Southern University of Science and Technology (Shenzhen, China), with high- and low-resolution reversal field increments, using an 8600 Series VSM (LakeShore Cryotronics) and processing data with VARIFORC (Egli, 2013) and FORCinel (Harrison & Feinberg, 2008). FORC measurement and processing parameters are given in Supporting Information S1.

3. Results

Figures 1d and 1e shows partial κ-T curves to ~340°C of two samples from the DE11 basalt. Both display a hump in heating and cooling curves. The maximum temperature was chosen as low as possible to avoid magneto-mineralogical changes, but high enough to display the hump. During the first cycle, κ increased by about 40%, peaking at ~290°C, then decreased again by ~20% at ~340°C. After cooling, κ was ~20% (powder sample) to ~40% (pebble sample) higher compared to the starting value. The second partial cycle also displayed a clearly irreversible behavior, returning to about the same κ-value after cooling. Remarkably, for both samples, this thermal hysteresis behavior was very similar in a subsequent third partial cycle.

The DE04 basalt also showed a hump-shaped κ-T curve during first heating to ~340°C, with κ increasing by ~60%, peaking at ~280°C (Figure 1f); however, after cooling, κ underscored the starting value by ~10%. In the second cycle to ~340°C, a reversible behavior occurred, and the hump peak shifted to ~40°C higher temperature. Two additional cycles revealed the same behavior, and the hump became clearer because of the higher maximum temperature (~390°C).

The M_s-T curves of DE11 (sample pre-heated to ~340°C in argon) neither showed a hump nor a slope anomaly due to maghemite inversion (Figure 1c). The first two partial cycles were nearly identical and reversible. The minor thermal hysteresis in the first cycle might be due to the external field (135 mT) that does not completely saturate magnetite. After heating to ~700°C (3rd cycle), the M_s-value strongly increased, similar to the full κ-T cycles. The partial 4th cycle nearly followed the 3rd cycle's cooling curve.

Additional partial κ-T cycles were conducted on a pre-heated pebble sample of the DE11 basalt, varying peak fields and heating rates (Figures 2a–2f). The κ-values increased slightly cycle by cycle, totaling by ~10%. No systematic differences appeared for different external fields, but a faster heating rate decreased the gap between heating and cooling curves (Figures 2d–2f).

High-resolution FORC diagrams of the DE11 basalt and the red soil (Figures 3a and 3b display a central ridge along the B_c-axis and a vertical ridge at zero B_c. The central ridge is surrounded by an oval structure. The FORC

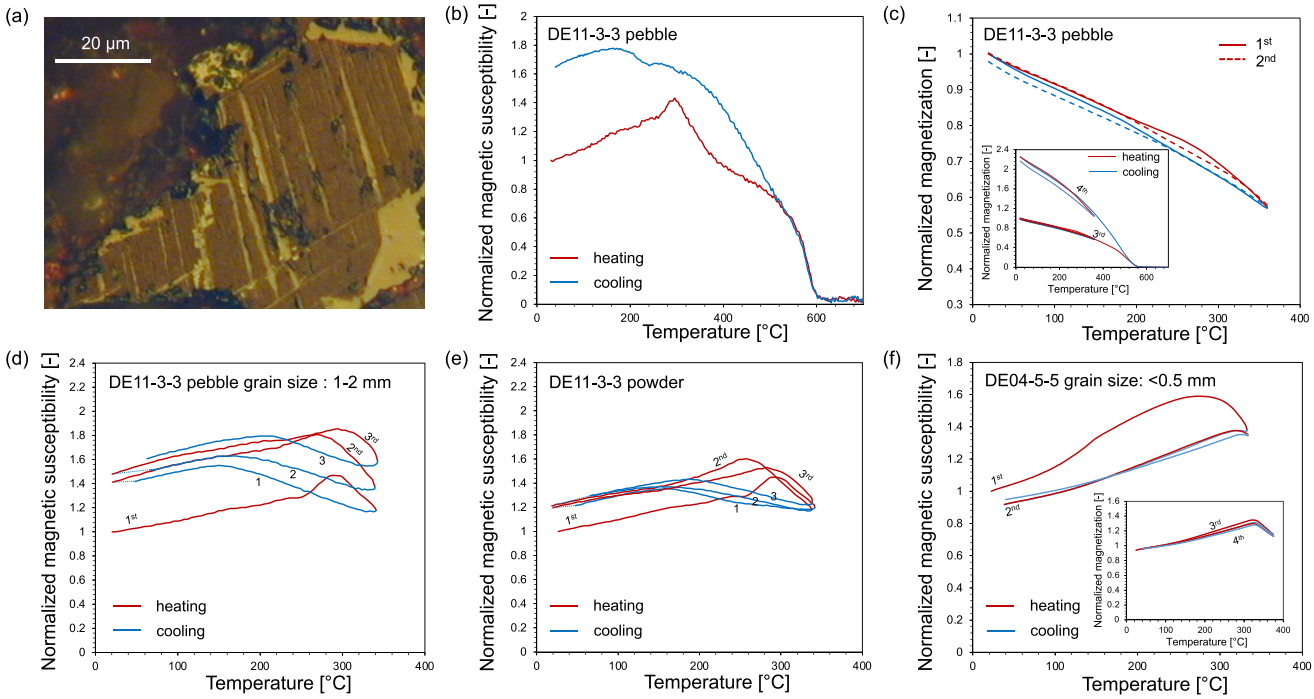

Figure 1. (a) Optical micrograph of the DE11 basalt with typical magnetite-ilmenite lamellae (magnetite revealed by dark ferrofluid coverage); (b) κ-T cycling to ~700°C of DE11; for methods of (a, b) see Zhang, Appel, Basavaiah, et al. (2021). (c) DE11 partial M_s-T curves (sample pre-heated to ~340°C before 1st cycle; insert: cycle 3–~700°C and partial cycle 4) (d–f) Partial κ-T curves of DE11 (d, e) and DE04 (f; insert: 3rd and 4th cycles to ~40°C higher) basalts, external peak field 200 A/m, heating rate of ~12°C/min (original samples used for 1st cycles).

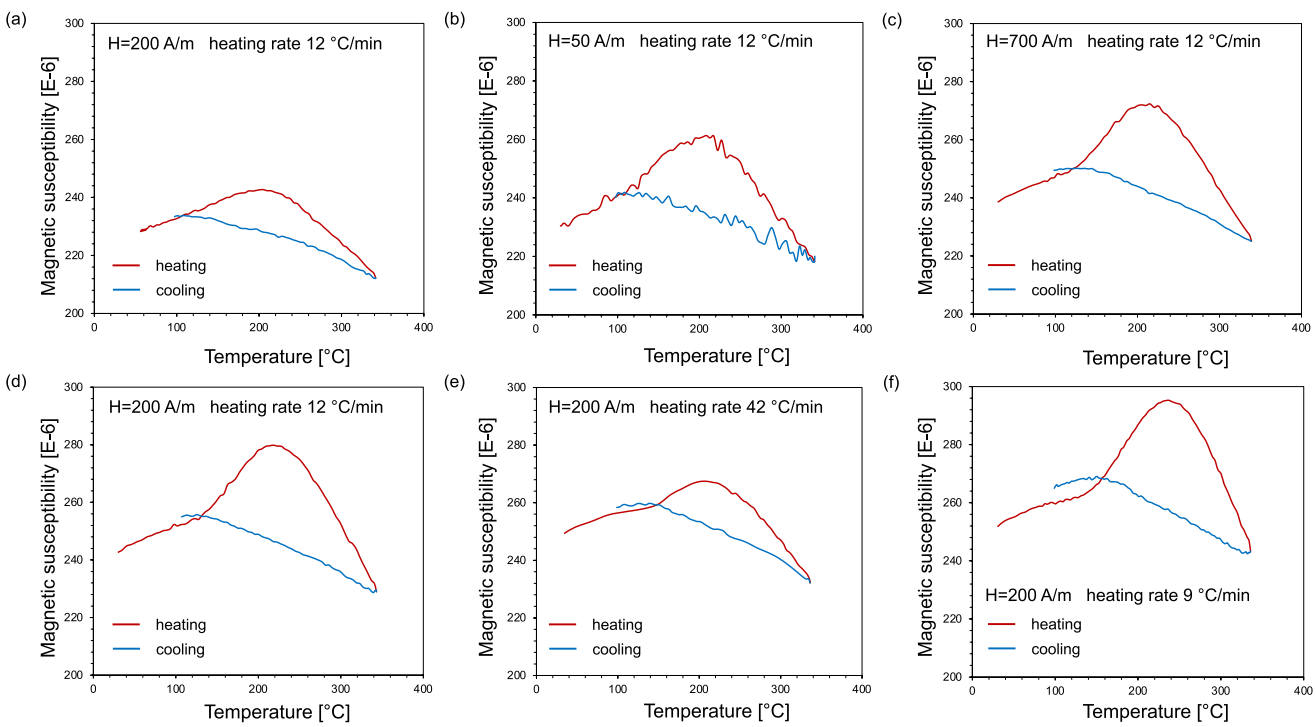

Figure 2. (a–f) Partial κ-T cycles for DE11 (1-2 mm-sized pebble sample DE11-3-3; sample twice pre-heated to ~340°C in argon before the experiment), measured in the order (a) to (f), at different external fields (H) and heating rates (same scale used for all six plots, to document the slight κ-increase cycle by cycle; note: κ-scale not from zero).

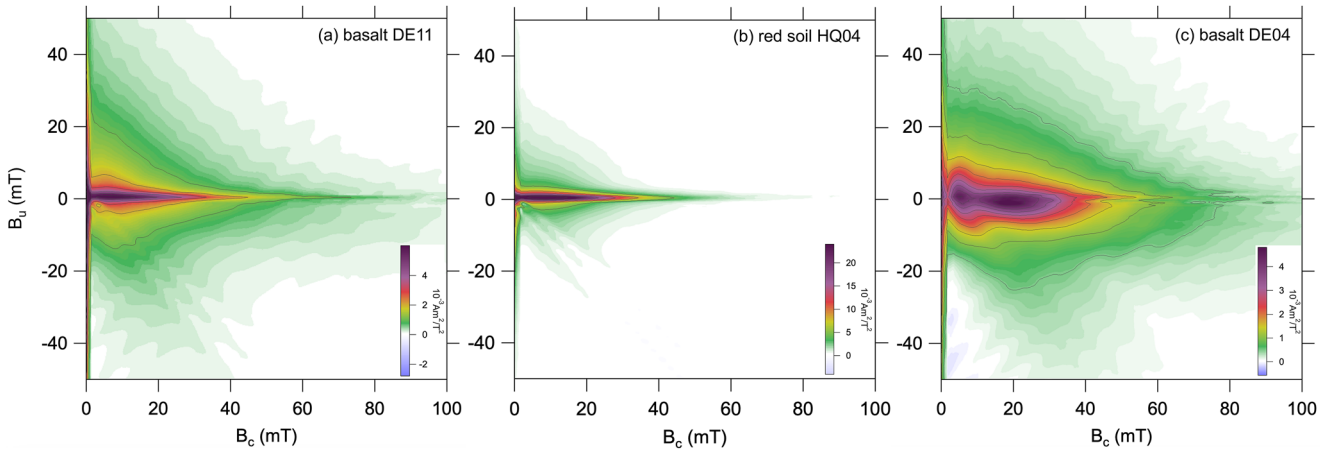

Figure 3. High-resolution FORC diagrams for original samples of the basalts DE11 (a) and DE04 (c), and the red soil (b). For detailed measurement and processing parameters see Supporting Information S1. Uniform B_c and B_u scaling is used for easier comparison. Features along the descending diagonal in (a) and (b) are probably smoothing artifacts.

diagram of the DE04 basalt (Figure 3c) reveals a vertical ridge and an oval structure along B_c with two centers, but a clear central ridge is missing. At low FORC function values there is a diverging signature toward the B_u-axis for all three samples.

Figure 4 shows κ-T results of the DE11 basalt and the red soil, with partial κ-T cycles to ~340°C (cycles 1&2), followed by a 3rd cycle to ~700°C, and a 4th cycle to ~340°C. The cooling curve after heating to ~700°C cycles plots at a much higher κ-level, the hump broadened and shifted to higher temperature. Low-resolution FORC diagrams (Figure 4) trace the domain state before and after the κ-T cycles. The vertical ridge, which is clearly seen in Figure 3, can only be faintly guessed due to the low resolution. No significant changes in the FORC diagrams were observed after partial heating to 340°C. After heating to ~700°C, the central ridge shifted to higher B_c-values. Differences in the red soil results were a decrease of ~15% in κ after the first cycle (DE11 basalt: ~15% increase) and a much larger increase of κ after cooling from ~700°C.

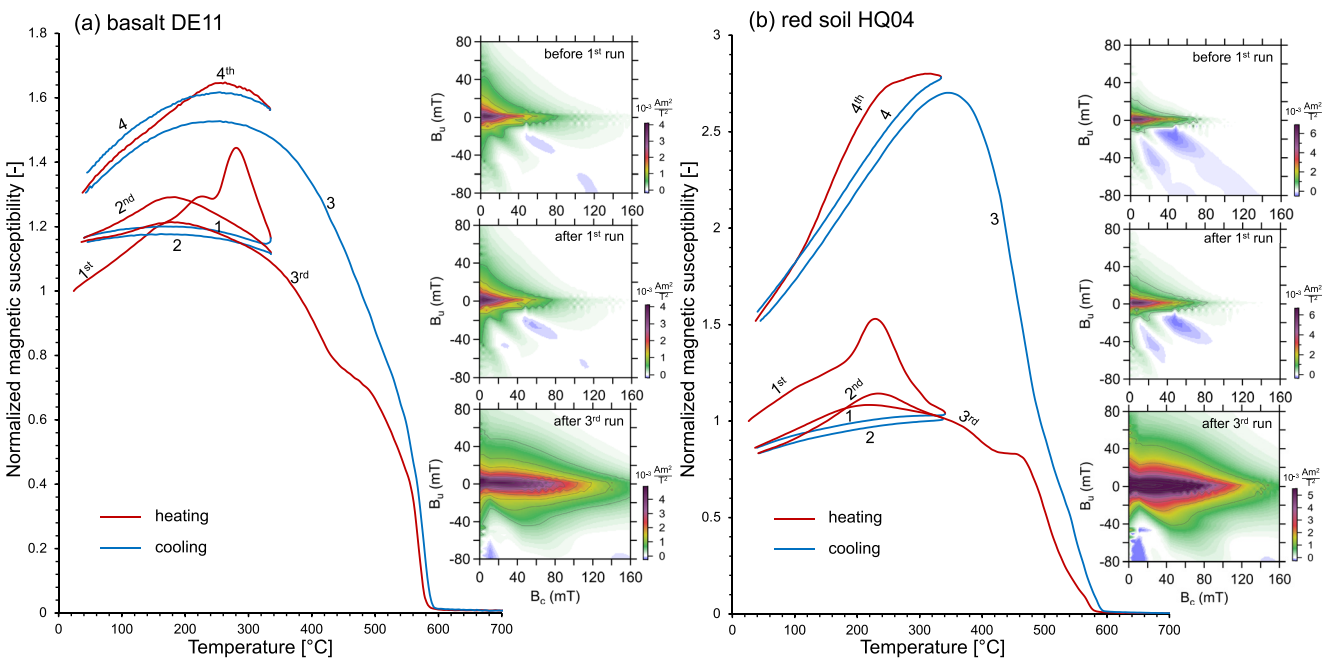

Figure 4. Thermomagnetic κ-T cycles and low-resolution FORC diagrams (for detailed measurement and processing parameters see Supporting Information S1) for (a) the DE11 basalt and (b) for a red soil sample: Partial cycles to ~340°C for the original sample (1st cycle), subsequent repetition to ~340°C (2nd cycle), followed by cycling to ~700°C (3rd cycle), and another partial cycle to ~340°C (4th cycle) after cooling from ~700°C. Uniform B_c and B_u scaling is used for easier comparison.

Overall, the results indicate a possible variation of the hump-peak position in heating curves of at least ~100°C. In subsequent partial cycles of the same sample (Figure 2a–2f) peak temperatures in heating curves varied by ~30°C. Cooling curves also showed a hump shape, however, with a smaller peak amplitude and a peak position at up to more than 100°C lower temperature.

4. Discussion

The experimental results are robust evidence for a significant and largely repeatable thermal hysteresis in the κ-T behavior of the DE11 basalt, which one may call a "reversible irreversible effect" (RIE). Occurrence of the RIE precludes that the decreasing slope during heating is caused by the inversion of maghemite or the presence of Ti-rich titanomagnetite, which is moreover rejected by the reversible and smooth variation of M_s-T curves. This does not exclude irreversible changes in the magnetic state of large crystals or SP particle aggregates, which affect κ but not M_s. In the discussion below, we focus on (a) the origin of the hump and the identification of particles expected to be responsible for the hump, (b) the possible mechanism of the thermal hysteresis, and (c) the impact on the interpretation of κ-T curves. We primarily use the results of the DE11 basalt, and employ the results of the red soil HQ04 and the DE04 basalt when it is important for comparison.

4.1. Origin and Principle Features of Hump-Shaped κ-T Curves

The theoretical temperature dependence of the in-phase susceptibility (measured by the MFK1) of non-interacting single-domain particles is based on the equation (Egli, 2009; Worm, 1998):

$$\kappa = \kappa_{SSD} + \frac{\mu_0 V {M_s}^2}{3 k_B T} \cdot \frac{1}{1 + \omega^2 \tau^2} \quad (1)$$

The second term in Equation 1 predicts a hump-shaped κ-T curve for thermal relaxation around the SSD-SP transition. Parameters are temperature T, particle volume V, saturation magnetization M_s, angular frequency ω of the applied field, relaxation time τ, and SSD susceptibility κ_{SSD} (k_B: Boltzmann constant; μ_0: free-space magnetic permeability). The τ-value derives from $\tau_0 \exp(K_{eff} V/(k_B T))$ (Néel, 1949), where K_{eff} is the effective anisotropy energy density ($\tau_{0:}$ spin relaxation time). For $\tau \rightarrow \infty$, κ approaches to $\kappa_{SSD} = (2/3)\ M_s/H_k$ (Stoner & Wohlfarth, 1948) (H_k: microcoercivity). For larger particle volume, the hump-peak occurs at higher temperatures (Worm, 1998; Zhao & Liu, 2010), which indicates that the observed shift of the hump-peak to higher temperature after 700°C heating (Figure 4) and after the first partial heating of DE04 (Figure 1f) reflects an increase of the effective particle size.

For interpreting the FORC diagrams, we follow Roberts et al. (2014) and Egli (2021). The FORC characteristics (Figure 3) confirm that the original samples indeed contain the type of magnetite particles expected to cause a hump. Generally, a single-domain fraction is dominating, which for the red soil sample agrees with physical particle sizes (~5–20 nm) shown by TEM observations (Figure S2b in Supporting Information S1; Zhang et al., 2020). In the basalts, fine particle behavior may result from small-scale lamellar structures (Figures S2a and S2c in Supporting Information S1; Zhang, Appel, Basavaiah, et al., 2021), and from particle-internal stress. Heterogenous stresses due to variable maghemitization (Béguin & Fabian, 2021; Hodych, 1982) and lamellar intersections (ter Maat et al., 2020) could segment particles into sub-regions, similar to Ti-rich titanomagnetites (Appel & Soffel, 1984). In the following, speaking of "particles" refers to physical particles (red soil), but also structures behaving like fine particles such as lamellar magnetite and stress-induced sub-regions inside them.

High-resolution FORC diagrams of the original DE11 basalt and the red soil samples (Figures 3a and 3b) display similar features. The central ridge along the B_c-axis is typical for the presence of non- or weakly-interacting SSD particles. The oval structure around the central ridge indicates significant magnetic interaction in part of the magnetite fraction. Although in the red soil the nanoparticles are arranged in clusters (Figure S2b in Supporting Information S1), interparticle coupling appears to be weaker than for DE11, as indicated by the relatively small B_u-extent of the oval structure. This is probably due to partial or complete oxidization of part of the nanoparticles to hematite (Zhang et al., 2020), which does not directly influence the FORC data, but increases distances between magnetite nanoparticles. The vertical ridge at zero B_c reflects viscous behavior likely caused by thermally activated SP particles. The peak of the central ridge near zero B_c indicates that the central and vertical ridges are connected, probably reflecting a related spectrum of SSD and SP particles. For the DE04 basalt, a similar group

of particles is indicated by the vertical ridge and the lower B_c-component of the bimodal oval structure, while the higher B_c-component may be associated with a larger sized SSD fraction (Figure 3c). The diverging distribution at low FORC function values, which occurs in all three samples, could represent particles with vortex spin configurations or other pseudo-single domain particles, or may stem from interacting single-domain particles (Egli, 2006).

Equation 1 and the FORC results explain the hump, but not the thermal hysteresis. The hysteresis behavior is clearly a true physical effect. The influence of heat capacities can be ruled out as the hysteresis at a faster heating rate is significantly smaller than for slower heating-cooling (Figures 2e and 2f). According to Equation 1, a thermal hysteresis would result when the size distribution varies differently during heating and cooling. Reversible variation of the physical particle size is of course unrealistic, but such reasoning suggests that the collective behavior of coupled single-domain particles could play a crucial role in the thermal variation of κ.

4.2. Origin of the Thermal Hysteresis

Petracic et al. (2006) proposed collective freezing of nanoparticle clusters into superferromagnetic behavior through dipolar interaction at high packing of SP ($Co_{80}Fe_{20}$) particles. For the studied basalts and the red soil, SP particles are indicated by the vertical ridge in the FORC diagrams (Figure 3). Frequency dependence k_{fd}% (measured at 976 Hz and 16 kHz) indicates that the relative SP proportion is extremely high (~18%) for the red soil (Zhang et al., 2020), relatively high (~9%) for DE11 and still significant (~7.5%) for DE04 (Zhang, Appel, Basavaiah, et al., 2021).

A thermal hysteresis due to irreversible arrangements of coupled nanoparticle moments was modeled in previous studies, based on iron nano-dots exchange-coupled to a layer with fixed spin directions (Dantas et al., 2007), or dipolar coupling in clusters of gadolinium SP particles (Souza et al., 2019). In these studies, a direct external field was considered, yet with more than one order higher fields compared to the peak field applied in the MFK1. An experimental thermal hysteresis acquired in an alternating external field was reported by Liubimova et al. (2017) for dysprosium, and was explained by the stabilization of a residual ferromagnetic phase by lattice defects.

The local field at each nanoparticle is the sum of the external field and dipolar fields of neighboring particles (Souza et al., 2019). The size and positioning of nanoparticles have a strong effect on cluster behavior (Pedrosa et al., 2018). Clustering may lead to reduction of κ, but for external fields parallel to the major cluster axis, κ can be larger than for individual nanoparticles (Pedrosa et al., 2018). Based on theoretical models, Pedrosa et al. (2018) found that κ increases with decreasing distance of SP particles in elliptical clusters, due to anisotropic dipolar fields. They showed that coupled nanoparticle moments can be stable in varying external fields, but low external field changes of few hundred A/m can also cause large magnetization changes. In natural samples, particles typically exist in variable sizes, often aggregated in clusters of SP and SSD particles with anisotropic dipolar fields comparable to the settings of Souza et al. (2019), Dantas et al. (2007) and Liubimova et al. (2017). In part of these clusters, the dipolar coupling could be outweighed by the external field of the MFK1, causing changes in the directional arrangement of particle moments.

We hypothesize that the thermal hysteresis of the studied samples results from dipolar coupling effects, which based on Pedrosa et al. (2018) can modulate the hump-shaped thermal dependency of thermal relaxation, without eliminating SP characteristics of the individual particles (Andersson et al., 2016; Chen et al., 2008; Schmool & Kachkachi, 2016; Souza et al., 2019). Thus, a hump in κ-T curves could exist even in samples where all particles are coupled.

Dantas et al. (2007) argued that superferromagnetic behavior decays with reduction of the interaction field, causing a thermal hysteresis. The decrease of M_s with heating will weaken the dipolar coupling field (Souza et al., 2019), which is equivalent to an increasing distance between particles. According to Pedrosa et al.'s (2018) results, the weakening of dipolar coupling causes a tendency toward lower κ compared to non-interacting particles. Configurations in clusters with lower κ, formed at the maximum temperature, may be partly preserved in local energy minima states during cooling, similar to spin vortex states in single-domain particles (Fabian et al., 1996; Williams & Dunlop, 1989), which could explain why the cooling curve runs below the heating curve after switching to cooling.

4.3. Impact on Interpreting κ-T Curves

The results demonstrate that a hump in κ-T curves is related to thermal relaxation of single-domain magnetite particles. The experimental observation of an RIE is a robust result, whereas the proposed mechanism for the RIE is a hypothesis for the time being.

FORC distributions after cycling to 700°C extend to higher B_c compared to the original samples (Figure 4), indicating an increase in the proportion of single-domain particles above the size of thermal relaxation. According to the theoretical relationship between the hump-peak position and the particle volume (Zhao & Liu, 2010), the observed shift of the hump-peak to a higher temperature after 700°C cycling (Figure 4) suggests that heating can shift the domain state toward larger effective particle sizes. The peak-shift for DE04 (Figure 1f) after the first partial cycle indicates that the effective particle size can also change at lower temperature. In addition, the κ-T results in Figures 1f and 4 show that as the effective particle size increases, the thermal hysteresis can weaken or disappear. The cause of the effective size change is still unclear. We assume that it is due to the welding of particle interfaces (Bedanta et al., 2015), or the homogenization of internal stresses.

Both M_s and κ increased after 700°C heating (Figures 1b, 1c and 4). For the red soil, this may be due to the reduction of hematite to magnetite; however, there is no plausible mineralogical transition for neo-formation of magnetite in DE11. Higher M_s could result from stress reduction leading to a higher degree of saturation in the 135 mT field. Moreover, nanoparticles have a lower M_s than bulk magnetite (Li et al., 2017), and hence M_s may grow with an increase in the effective particle size. The increase of κ could be largely related to stress healing and to the increase of the effective particle size with the corresponding change in the thermal relaxation behavior.

A higher κ value in the first cycle after cooling to room temperature (Figures 1d and 1e) and the slight increase of κ in subsequent partial cycles (Figure 2a–2f) can be explained by the healing of internal stresses (Kontny & Grothaus, 2017; Van Velzen & Dekkers, 1999b). Reduction of stress anisotropy decreases the effective anisotropy energy density K_{eff}, and in turn, lowers τ in Equation 1, while magnetocrystalline and shape anisotropies remain unchanged after κ-T cycling. In samples, where heating leads to partial oxidation of magnetite, the effect of stress healing can be masked. The κ-value in the thermal hysteresis of DE04 (Figure 1f) and the red soil (Figure 4b) after the first partial cycle is lower compared to the initial value, which may reflect a partial loss of magnetite. The absence of thermal hysteresis in the hump of the second cycle of DE04 supports that SP particles, which are assumed to be depleted during the first partial heating by an increase of the effective particle size or by oxidation, play an important role in the thermal hysteresis behavior.

The studied samples DE11 and DE04 represent basalts with lamellar magnetite-ilmenite, which are widespread and of great interest. Moreover, a hump and an RIE could occur in various natural materials, as shown by the results of the red soil sample (Figure 4b). Depending on the grain size distribution and other effects such as internal stresses, the hump shape and hump-peak position can vary greatly. Through superposition by a multidomain fraction or magnetic mineralogy changes, the hump and an RIE may be overlooked despite a significant SP and SSD fraction in the sample, in particular when the amplitude of the hump is damped due to interaction fields in particle clusters. The thermal hysteresis still holds unexplored potential for magnetic granulometry and the understanding of particle interaction, and thus merits further investigation.

5. Conclusions

The results are a warning that interpreting a marked decrease in κ-T curves at intermediate temperatures by maghemite inversion might not always be correct. Instead, single-domain magnetite undergoing the SSD to SP transition should be considered when a hump is detected. A significantly different hump shape in cooling curves after heating to 700°C may reflect a change in effective particle sizes. Reversible thermal hysteresis behavior in repeated partial κ-T cycles can be considered as a hint of interaction effects in clusters of magnetite particles, with particular importance of an SP fraction. Irreversible heating-cooling behavior is thus not always related to changes in magnetic mineralogy.

Data Availability Statement

Experimental data in this manuscript are available on Mendeley for public download at http://dx.doi.org/10.17632/zx7y6g9rdv.2.

Acknowledgments
We thank Adrian Höfken and Tilo von Dobeneck for enabling and measuring M_s-T curves; Udo Neumann for instructions in optical microscopy; Nathani Basavaiah and Shouyun Hu for helping in the field; Qingsong Liu and Yu-Min Chou for supporting the measurement opportunity and for valuable discussions. Two reviewers (Ramon Egli and anonymous) provided very helpful comments to improve the manuscript. The work was supported by the National Natural Science Foundation of China (42204082) and the German Research Foundation (AP 34/44-1). QZ and EA participated in both experimental observations (led by QZ) and interpretation (led by EA). Open Access funding enabled and organized by Projekt DEAL. Qi Zhang and Erwin Appel contributed equally to this work.

References

Ahmed, I. A. M., & Maher, B. A. (2018). Identification and paleoclimatic significance of magnetite nanoparticles in soils. *Proceedings of the National Academy of Sciences*, *115*(8), 1736–1741. https://doi.org/10.1073/pnas.1719186115

Andersson, M. S., De Toro, J. A., Lee, S. S., Normile, P. S., Nordblad, P., & Mathieu, R. (2016). Effects of the individual particle relaxation time on superspin glass dynamics. *Physical Review B*, *93*(5), 054407. https://doi.org/10.1103/PhysRevB.93.054407

Appel, E., & Soffel, H. C. (1984). Model for the domain state of Ti-rich titanomagnetites. *Geophysical Research Letters*, *3*, 189–192. https://doi.org/10.1029/GL011i003p00189

Appel, E., & Soffel, H. C. (1985). Domain state of Ti-rich titanomagnetites deduced from domain structure observations and susceptibility measurements. *Journal of Geophysics*, *56*, 121–132.

Bedanta, S., Seki, T., Iwama, H., Shima, T., & Takanashi, K. (2015). Superferromagnetism in dipolarly coupled $L1_0$ FePt nanodots with perpendicular magnetization. *Applied Physics Letters*, *107*(15), 152410. https://doi.org/10.1063/1.4933381

Béguin, A., & Fabian, K. (2021). Demagnetization energy and internal stress in magnetite from temperature dependent hysteresis measurements. *Geophysical Research Letters*, *48*(24), e2021GL096147. https://doi.org/10.1029/2021GL096147

Chen, D. X., Sanchez, A., Xu, H., Gu, H. C., & Shi, D. L. (2008). Size-independent residual magnetic moments of colloidal Fe_3O_4-polystyrene nanospheres detected by ac susceptibility measurements. *Journal of Applied Physics*, *104*(9), 093902. https://doi.org/10.1063/1.3005988

Dantas, A. L., Silva, A. S. W. T., Rebouças, G. O. G., Carriço, A. S., & Camley, R. E. (2007). Thermal hysteresis of interface biased ferromagnetic dots. *Journal of Applied Physics*, *102*(12), 123907. https://doi.org/10.1063/1.2827478

Deng, C. L., Zhu, R. X., Jackson, M. J., Verosub, K. L., & Singer, M. J. (2001). Variability of the temperature-dependent susceptibility of the Holocene eolian deposits in the Chinese Loess Plateau: A pedogenesis indicator. *Physics and Chemistry of the Earth, Part A: Solid Earth and Geodesy*, *26*(11–12), 873–878. https://doi.org/10.1016/S1464-1895(01)00135-1

Deng, C. L., Zhu, R. X., Verosub, K. L., Singer, M. J., & Vidic, N. J. (2004). Mineral magnetic properties of loess/paleosol couplets of the Central Loess Plateau of China over the last 1.2 Myr. *Journal of Geophysical Research*, *109*(B1), B01103. https://doi.org/10.1029/2003JB002532

Deng, C. L., Zhu, R. X., Verosub, K. L., Singer, M. J., & Yuan, B. Y. (2000). Paleoclimatic significance of the temperature-dependent susceptibility Holocene loess along a NW-SE transect in the Chinese Loess Plateau. *Geophysical Research Letters*, *27*(22), 3715–3718. https://doi.org/10.1029/2000GL008462

Dunlop, D. J. (2014). High-temperature susceptibility of magnetite: A new pseudo-single-domain effect. *Geophysical Journal International*, *199*(2), 707–716. https://doi.org/10.1093/gji/ggu247

Dunlop, D. J., & Özdemir, Ö. (1997). *Rock magnetism: Fundamentals and frontiers*. Cambridge Studies in Magnetism (p. 573). Cambridge University Press.

Egli, R. (2006). Theoretical aspects of dipolar interactions and their appearance in first-order reversal curves of thermally activated single-domain particles. *Journal of Geophysical Research*, *111*(B12), B12S17. https://doi.org/10.1029/2006JB004567

Egli, R. (2009). Magnetic susceptibility measurements as a function of temperature and frequency, 1. Inversion theory. *Geophysical Journal International*, *177*(2), 395–420. https://doi.org/10.1111/j.1365-246X.2009.04081.x

Egli, R. (2013). VARIFORC: An optimized protocol for the calculation of non-regular first-order reversal curve (FORC) diagrams. *Global and Planetary Change*, *110*, 302–320. https://doi.org/10.1016/j.gloplacha.2013.08.003

Egli, R. (2021). Magnetic characterization of geologic materials with first-order reversal-curves. In V. Franco & B. Dodrill (Eds.), *Magnetic measurement techniques for materials characterization* (pp. 455–604). Springer Nature Publishing Group. https://doi.org/10.1007/978-3-030-70443-8_17

Fabian, K., Kirchner, A., Williams, W., Heider, F., Leibl, T., & Hubert, A. (1996). Three-dimensional micromagnetic calculations for magnetite using FFT. *Geophysical Journal International*, *124*(1), 89–104. https://doi.org/10.1111/j.1365-246X.1996.tb06354.x

Harrison, R. J., & Feinberg, J. M. (2008). FORCinel: An improved algorithm for calculating first-order reversal curve distributions using locally weighted regression smoothing. *Geochemistry, Geophysics, Geosystems*, *9*(5), Q05016. https://doi.org/10.1029/2008GC001987

Hodych, J. P. (1982). Magnetostrictive control of coercive force in multidomain magnetite. *Nature*, *298*(5874), 542–544. https://doi.org/10.1038/298542a0

Kontny, A., & Grothaus, L. (2017). Effects of shock pressure and temperature on titanomagnetite from ICDP cores and target rocks of the El'gygytgyn impact structure, Russia. *Studia Geophysica et Geodaetica*, *61*(1), 162–183. https://doi.org/10.1007/s11200-016-0819-3

Li, Q., Kartikowati, C. W., Horie, S., Ogi, T., Iwaki, T., & Okuyama, K. (2017). Correlation between particle size/domain structure and magnetic properties of highly crystalline Fe_3O_4 nanoparticles. *Scientific Reports*, *7*(1), 9894. https://doi.org/10.1038/s41598-017-09897-5

Liu, Q. S., Deng, C. L., Yu, Y. J., Torrent, J., Jackson, M. J., Banerjee, S. K., & Zhu, R. X. (2005). Temperature dependence of magnetic susceptibility in an argon environment: Implications for pedogenesis of Chinese loess/palaeosols. *Geophysical Journal International*, *161*(1), 102–112. https://doi.org/10.1111/j.1365-246X.2005.02564.x

Liubimova, I., Corró Moyà, M. L., Torrens-Serra, J., Recarte, V., Pérez-Landazábal, J. I., & Kustov, S. (2017). Low field magnetic and thermal hysteresis in antiferromagnetic dysprosium. *Metals*, *7*(6), 215. https://doi.org/10.3390/met7060215

Néel, L. (1949). Théorie du traînage magnétique des ferromagnétiques en grains fins avec applications aux terres cuites. *Annales Geophysicae*, *5*, 99–136.

Pedrosa, S. S., Martins, S. M. S. B., Jr., Souza, R. M., Dantas, J. T. S., Souza, C. M., Rebouças, G. O. G., et al. (2018). Dipolar effects on the magnetic phases of superparamagnetic clusters. *Journal of Applied Physics*, *123*(23), 233902. https://doi.org/10.1063/1.5030739

Petracic, O., Chen, X., Bedanta, S., Kleemann, W., Sahoo, S., Cardoso, S., & Freitas, P. P. (2006). Collective states of interacting ferromagnetic nanoparticles. *Journal of Magnetism and Magnetic Materials*, *300*(1), 192–197. https://doi.org/10.1016/j.jmmm.2005.10.061

Petrovský, E., & Kapička, A. (2006). On determination of the Curie point from thermomagnetic curves. *Journal of Geophysical Research*, *111*(B12), B12S27. https://doi.org/10.1029/2006JB004507

Ramdohr, P. (1980). *The ore minerals and their intergrowths* (2nd ed., p. 1207). Pergamon Press, University of California.

Roberts, A. P., Heslop, D., Zhao, X., & Pike, C. R. (2014). Understanding fine magnetic particle systems through use of first-order reversal curve diagrams. *Reviews of Geophysics*, *52*(4), 557–602. https://doi.org/10.1002/2014RG000462

Schmool, D. S., & Kachkachi, H. (2016). Chapter one - collective effects in assemblies of magnetic nanoparticles. *Solid State Physics*, *67*, 1–101. https://doi.org/10.1016/bs.ssp.2016.08.001

Souza, C. M., Pedrosa, S. S., Carriço, A. S., Rebouças, G. O. G., & Dantas, A. L. (2019). Thermal hysteresis of superparamagnetic Gd nanoparticle clusters. *Physical Review, B*, *99*(17), 174441. https://doi.org/10.1103/PhysRevB.99.174441

Stoner, E. C., & Wohlfarth, E. P. (1948). A Mechanism of magnetic hysteresis in heterogeneous alloys. *Philosophical Transactions of the Royal Society of London - Series A: Mathematical and Physical Sciences*, *240*, 599–642.

ter Maat, G. W., Fabian, K., Church, N. S., & McEnroe, S. A. (2020). Separating geometry- from stress-induced remanent magnetization in magnetite with ilmenite lamellae from the Stardalur basalts, Iceland. *Geochemistry, Geophysics, Geosystems*, *21*(2), e2019GC00876. https://doi.org/10.1029/2019GC008761

Vahle, C., & Kontny, A. (2005). The use of field dependence of AC susceptibility for the interpretation of magnetic mineralogy and magnetic fabrics in the HSDP-2 basalts, Hawaii. *Earth and Planetary Science Letters*, *238*(1–2), 110–129. https://doi.org/10.1016/j.epsl.2005.07.010

van Velzen, A. J., & Dekkers, M. J. (1999a). The incorporation of thermal methods in mineral magnetism of loess-paleosol sequences: A brief overview. *Chinese Science Bulletin*, *44*(Supp. 1), 53–63. https://doi.org/10.1360/sb1999-44-S1-53

van Velzen, A. J., & Dekkers, M. J. (1999b). Low-temperature oxidation of magnetite in loess-paleosol sequences: A correction of rock magnetic parameters. *Studia Geophysica et Geodaetica*, *43*(4), 357–375. https://doi.org/10.1023/A:1023278901491

Wang, B., Xia, D. S., Yu, Y., Jia, J., Nie, Y., & Wang, X. (2015). Detecting the sensitivity of magnetic response on different pollution sources - a case study from typical mining cities in northwestern China. *Environmental Pollution*, *207*, 288–298. https://doi.org/10.1016/j.envpol.2015.08.041

Williams, W., & Dunlop, D. J. (1989). Three-dimensional micromagnetic modelling of ferromagnetic domain structure. *Nature*, *337*(6208), 634–637. https://doi.org/10.1038/337634a0

Worm, H. U. (1998). On the superparamagnetic-stable single domain transition for magnetite, and frequency dependence of susceptibility. *Geophysical Journal International*, *133*(1), 201–206. https://doi.org/10.1046/j.1365-246X.1998.1331468.x

Zhang, Q., Appel, E., Basavaiah, N., Hu, S. Y., Zhu, X. H., & Neumann, U. (2021). Is alteration of magnetite during rock weathering climate-dependent? *Journal of Geophysical Research: Solid Earth*, *126*(10), e2021JB022693. https://doi.org/10.1029/2021JB022693

Zhang, Q., Appel, E., Hu, S. Y., Pennington, R. S., Meyer, J., Neumann, U., et al. (2020). Nano-magnetite aggregates in red soil on low magnetic bedrock, their change during source-sink transfer and implications for paleoclimate studies. *Journal of Geophysical Research: Solid Earth*, *125*(10), e2020JB020588. https://doi.org/10.1029/2020JB020588

Zhang, Q., Appel, E., Stanjek, H., Byrne, J. M., Berthold, C., Sorwat, J., et al. (2021). Humidity related magnetite alteration in an experimental setup. *Geophysical Journal International*, *224*(1), 69–85. https://doi.org/10.1093/gji/ggaa394

Zhao, X. Y., & Liu, Q. S. (2010). Effects of the grain size distribution on the temperature-dependent magnetic susceptibility of magnetite nanoparticles. *Science China Earth Sciences*, *53*(7), 1071–1078. https://doi.org/10.1007/s11430-010-4015-y

Zhu, R. X., Lin, M., & Pan, Y. X. (1999). History of the temperature-dependence of susceptibility and its implications: Preliminary results along an E-W transect of the Chinese Loess Plateau. *Chinese Science Bulletin*, *44*(1), 81–86. https://doi.org/10.1360/sb1999-44-S1-81